This article has been accepted for publication in a future issue of this journal, but has not been fully edited. Content may change prior to final publication. Citation information: DOI 10.1109/TVT.2014.2381648, IEEE Transactions on Vehicular Technology

Unified Analysis of Low-SNR Energy Detection and Threshold Selection

Saman Atapattu, *Member, IEEE*, Chintha Tellambura, *Fellow, IEEE*, Hai Jiang, *Member, IEEE*, and Nandana Rajatheva, *Senior Member, IEEE*

***Abstract*—For spectrum sensing in cognitive radio networks, the IEEE 802.22 standard requires the detection of primary signals with a signal-to-noise ratio (SNR) as low as -20 dB and receiver sensitivity as low as -116 dBm. Under such low-SNR levels, the performance of a conventional energy detector is analyzed in this paper. The analysis includes novel expressions for missed-detection probability and area under the receiver operating characteristic (ROC) curve. Thus, a unified framework covering fading channels, square-law diversity combining and cooperative spectrum-sensing scenarios is developed. The detection threshold is optimized to minimize the total error rate subject to bounded false alarm and missed-detection probabilities, which outperforms traditional detection threshold selection. Numerical results and Monte-Carlo simulation results with the IEEE 802.22 sensing requirements are provided and discussed.**

***Index Terms*—Cognitive radio, energy detection, low-SNR, spectrum sensing, threshold selection.**

I. Introduction

BROADBAND wireless access using the television (TV) white space spectrum has been approved by the US Federal Communications Commission (FCC). Among the standardization efforts [1], the IEEE 802.22 wireless regional area network (WRAN), which is designed to operate in the vacant TV bands, brings broadband access not only to the WiFi devices but also to general mobile networks (e.g., micro-cells, pico-cells, or femto-cells), allowing the use of the cognitive radio on a non-interfering basis [2]–[4].

However, cognitive radio requires spectrum sensing for opportunistic spectrum access. If spectrum sensing fails, primary users will have interference. For this reason, IEEE 802.22 prescribes the false alarm and missed-detection probabilities be less than 0.1. Due to possible multipath fading and/or shadowing caused by high-rise buildings, it is required that secondary users should reliably detect primary signals (i.e., satisfying the two requirements on false alarm and missed-detection probabilities) with a very low signal-to-noise ratio (SNR), such as -20 dB SNR with a signal power of -116 dBm and a noise floor of -96 dBm [4]. Thus, spectrum sensing at *low SNR* is vital.

Fortunately, a wide array of spectrum sensing techniques such as energy detection, matched filter detection, cyclostationary feature detection, covariance based detection and others may be employed [5]–[19]. While those techniques perform well at moderate and high SNRs, low-SNR operation typically requires a large number of samples, which impacts the sensing and processing time. For example, IEEE 802.22 limits the maximal detection latency to 2 seconds which may include sensing time and subsequent processing time. This maximal time limit is critical at low-SNR spectrum sensing.

Although spectrum sensing techniques at moderate and high SNRs have been researched a lot [5]–[9], the low-SNR case remains relatively unexplored. This case is treated for a differential energy detection scheme of multi-carrier systems (e.g., orthogonal frequency division multiplexing [OFDM]) in [10], for multi-antenna detectors (which improve the robustness to noise uncertainty) in [11], [12], and for a covariance based detection in [13]. Moreover, low-SNR cooperative spectrum sensing techniques are considered for belief propagation in [14], for cyclostationary detection in [15], for optimal relaying scheme in [16], and for multi-antenna with a noise-uncertainty-free detector in [17]. These works consider a generalized likelihood ratio (GLR) detector, an alternative energy detector, a cyclostationary feature detector, or a covariance based detector, in which the operating SNR ranges from -30 dB to 0 dB.

To complement those studies, we focus on energy detection, which has low complexity and low cost compared to other spectrum sensing techniques such as matched filter detection, cyclostationary feature detection, etc. [20]. Before that, we briefly mention some of the limitations of the state-of-the-art energy detection research when applied to the low-SNR case.

- Average detection (or missed-detection) probability derivation: In [21], the distribution of test statistic under each hypothesis follows a gamma distribution. Its cumulative distribution function (CDF) expression includes an incomplete gamma function. Only Gaussian channels are considered in [21]. With this model, the average detection probability under any fading channel has not been derived in closed-form in the literature (probably because of difficulties in further analysis with the incomplete gamma function). In [6]–[8], [22], by modeling the test statistic with its exact distribution, the aver-

Manuscript received January 20, 2014; revised June 11, 2014 and October 28, 2014; accepted December 5, 2014. The associate editor coordinating the review of this paper and approving it for publication was Dr. L. Zhao. This work was supported by the Natural Science and Engineering Research Council (NSERC) of Canada. S. Atapattu was with the Department of Electrical and Computer Engineering, University of Alberta, Edmonton, AB, Canada T6G 2V4, and currently is with the Department of Electrical and Computer System Engineering, Monash University, Clayton, Victoria 3800, Australia (e-mail: saman.atapattu@monash.edu). C. Tellambura and H. Jiang are with the Department of Electrical and Computer Engineering, University of Alberta, Edmonton, AB, Canada T6G 2V4. (e-mail: chintha@ece.ualberta.ca, hai1@ualberta.ca). N. Rajatheva is with the Centre for Wireless Communications (CWC), Department of Communications Engineering, University of Oulu, Oulu 90570, Finland. (e-mail: rrajathe@ee.oulu.fi). Some preliminary results of this paper were presented in the IEEE International Conference on Communications (ICC) 2011.

This article has been accepted for publication in a future issue of this journal, but has not been fully edited. Content may change prior to final publication. Citation information: DOI 10.1109/TVT.2014.2381648, IEEE Transactions on Vehicular Technology

age detection probabilities $\overline{P_d}$ over fading channels are derived. These $\overline{P_d}$ expressions however include special functions, infinite-order derivatives, and/or infinite series. Thus, computational complexity increases rapidly with N, the number of samples. In the low-SNR case, however, N is several thousands, and thus, the resulting complexity is prohibitive. To reduce complexity, rather than using the exact distribution of the test statistic, an approximation can be used [21], [23]–[25]. But these works are limited to Gaussian channels. For the low-SNR energy detection, $\overline{P_d}$ is derived for Rayleigh fading [26], and for Nakagami fading [27] with an integral form.

- Threshold selection: Traditionally, the threshold is selected to guarantee a given false alarm probability (P_f). For this purpose, the inversion of the P_f expression is needed. Closed-form inversion however is not possible using results in [6]–[8], [21], [22]. This difficulty is heightened for IEEE 802.22 which additionally requires bounded missed-detection probability P_{md} and bounded P_f simultaneously. Although works in [28] and [29] perform Central Limit Theorem (CLT)-based threshold selection, they focus on non-fading scenarios only.

In summary, analytical tools specifically for low-SNR energy detector performance analysis and threshold selection over fading and/or shadowing channels may not be available.

Contributions: In this paper, we provide a rigorous unified performance analysis for conventional energy detection in the low-SNR regime. In particular, this paper makes the following contributions:

1) Missed-detection probability and Area Under receiver operating characteristic (ROC) Curve (AUC) for different fading and networking scenarios are derived, overcoming the aforementioned limitations (i.e., computational complexity).
2) Optimal threshold is formulated subject to bounded false-alarm and missed-detection probabilities. Approximate optimal threshold values are derived analytically.
3) Using the derived analytical results, numerical examples for the IEEE 802.22 requirements are presented. We show that these stringent low-SNR requirements can be achieved by sufficiently high number of samples and high sampling rate (MHz range). Moreover, cooperative sensing or diversity combining can help greatly.

The rest of this paper is organized as follows. Section II discusses energy detection, the system, low-SNR approximation, generalized SNR distribution, and the performance measures. Section III analyzes the missed-detection probability and AUC for low SNRs. Sections IV is devoted to the analysis of the optimal detection threshold. Section V presents numerical and simulation results, followed by concluding remarks in Section VI. Related proofs are provided in the Appendix. Some preliminary results of this paper have been presented in [30].

II. Energy Detection Preliminaries

Depending on whether the primary signal is present or not, the nth signal sample, $y(n) = \theta h s(n) + w(n)$ follows a binary hypothesis: $\mathcal{H}_0$ (signal absent, $\theta = 0$) and $\mathcal{H}_1$ (signal present, $\theta = 1$). Here, h, $s(n)$ and $w(n)$ denote the wireless channel gain, the nth primary signal sample and the nth additive white Gaussian noise (AWGN) sample, respectively. The test statistic is given as $\Lambda = \sum_{n=1}^{N} |y(n)|^2$, where N is the number of samples. If the test statistic is larger than threshold λ, the primary signal is deemed to be present, and it is absent otherwise.

The AWGN samples $w(n)$, $n = 1, 2, \cdots, N$, are assumed to be independent and identically distributed (i.i.d.) circularly symmetric complex Gaussian (CSCG) random variables with mean zero and variance $\mathbb{E}[|w(n)|^2] = \sigma_w^2$, where $\mathbb{E}[\cdot]$ stands for expectation, i.e., $w(n) \sim \mathcal{CN}(0, \sigma_w^2)$. We assume that the detector knows the noise power exactly with the help of a noise power estimation technique [31]. Due to space limitation, we cannot treat the case with noise uncertainty in detail in this paper. However, a limited discussion can be found in Section V-D.

For i.i.d. signal samples under $\mathcal{H}_1$, the following three signal models are widely used in the literature:

- **S1**: $y(n)$ is Gaussian with nonzero mean, i.e., for given channel gain h, $\mathbb{E}[y(n)] = hs(n)$ [6], and the received SNR can be defined as
$$\gamma_{\text{S1}} = \frac{|h|^2 \frac{1}{N} \sum_{n=1}^{N} |s(n)|^2}{\sigma_w^2}.$$
- **S2**: $s(n)$ is a CSCG random variable, $s(n) \sim \mathcal{CN}(0, \sigma_s^2)$, thus $y(n) \sim \mathcal{CN}(0, \sigma_w^2 + \sigma_s^2)$ [12], and the received SNR can be defined as $\gamma_{\text{S2}} = |h|^2 \sigma_s^2 / \sigma_w^2$.
- **S3**: $s(n)$ is a signal with zero mean and σ_s^2 variance (distribution may be unknown [13]), and thus, the received SNR is the same as γ_{S2}, i.e., $\gamma_{\text{S3}} = |h|^2 \sigma_s^2 / \sigma_w^2$.

For **S2** and **S3**, with sufficiently large number of samples, the signal variance can be written by using its sample variance as
$$\sigma_s^2 \approx \frac{1}{N} \sum_{n=1}^{N} |s(n)|^2 - \left(\frac{1}{N} \sum_{n=1}^{N} s(n) \right)^2.$$
If the sample mean goes to zero, i.e., $\left[\sum_{n=1}^{N} s(n) \right] / N \to 0$, then $\sigma_s^2 \approx \left[\sum_{n=1}^{N} |s(n)|^2 \right] / N$, and thus, the received SNRs under the three signal models are approximately equal, given as
$$\frac{|h|^2 \frac{1}{N} \sum_{n=1}^{N} |s(n)|^2}{\sigma_w^2}.$$
Thus, without loss of generality, we denote the SNR at the detector as γ (i.e., $\gamma = \gamma_{\text{S1}}, \gamma_{\text{S2}},$ or γ_{S3}) for the rest of this paper.

The distribution of Λ for given h can be modeled exactly for all three signal models, but not for **S3** under $\mathcal{H}_1$. Therefore, by using the CLT, the distribution of Λ given h can be approximated as a normal distribution for sufficiently large N as [25]

$$\Lambda | h \sim \begin{cases} \mathcal{N}\left(N\sigma_w^2, N\sigma_w^4\right) : \mathcal{H}_0 \\ \mathcal{N}\left(N\sigma_w^2(1+\gamma), N\sigma_w^4(1+2\gamma)\right) : \mathcal{H}_1 \text{ with } \textbf{S1} \\ \qquad \text{or } \textbf{S3} \text{ (with complex-valued phase-shift keying [PSK])} \\ \mathcal{N}\left(N\sigma_w^2(1+\gamma), N\sigma_w^4(1+\gamma)^2\right) : \mathcal{H}_1 \text{ with } \textbf{S2}. \end{cases} \quad (1)$$

This article has been accepted for publication in a future issue of this journal, but has not been fully edited. Content may change prior to final publication. Citation information: DOI 10.1109/TVT.2014.2381648, IEEE Transactions on Vehicular Technology

The probability density function (PDF) of Λ under $\mathcal{H}_0$, denoted $f_{\Lambda|\mathcal{H}_0}(x)$, and the PDF of Λ under $\mathcal{H}_1$, denoted $f_{\Lambda|\mathcal{H}_1}(x)$, can be derived from (1). Under the low-SNR assumption ($\gamma \ll 1$), the signal has little impact on the variance of the test statistic under $\mathcal{H}_1$. Thus, in the low-SNR regime, expression (1) can be accurately approximated for any of the three signal models as [26], [31]

$$\Lambda_{\text{low}}|h \sim \begin{cases} \mathcal{N}\left(N\sigma_w^2, N\sigma_w^4\right) & : \mathcal{H}_0 \\ \mathcal{N}\left(N\sigma_w^2(1+\gamma), N\sigma_w^4\right) & : \mathcal{H}_1. \end{cases} \tag{2}$$

While the exact P_f and P_{md} expressions are different for the three different signal models (**S1**, **S2**, and **S3**), the adoption of (2) permits a unified and accurate treatment for the three signal models, as follows. Thus, this approximation (2) is used for the rest of this paper.

Based on (2), the false alarm probability P_f and the missed-detection probability $P_{\text{md}}(\gamma)$ can be evaluated as

$$P_f = \frac{1}{2}\text{Erfc}\left(\frac{\lambda - N\sigma_w^2}{\sqrt{2N}\sigma_w^2}\right) \tag{3}$$

and

$$P_{\text{md}}(\gamma) \approx 1 - \frac{1}{2}\text{Erfc}\left(\frac{\lambda - N\sigma_w^2(1+\gamma)}{\sqrt{2N}\sigma_w^2}\right), \tag{4}$$

respectively, where $\text{Erfc}(\cdot)$ is the complementary error function [32] defined as $\text{Erfc}(z) = (2/\sqrt{\pi})\int_z^\infty e^{-t^2}dt$.

Since $P_{\text{md}}(\gamma)$ depends on channel gain, a generalized SNR distribution is necessary to derive analytical results valid for various cases with path loss, large-scale fading and/or small-scale fading. Thus, we use a mixture of gamma distributions [33] for γ

$$f_\gamma(x) = \sum_{i=1}^{S} \alpha_i x^{\beta_i - 1} e^{-\zeta_i x}, \quad x \geq 0,\ \alpha_i,\ \beta_i,\ \zeta_i > 0, \tag{5}$$

where S is the number of terms, α_i, β_i and ζ_i are parameters that represent the potential fading and shadowing effects, and $\sum_{i=1}^{S} \alpha_i \Gamma(\beta_i)\zeta_i^{-\beta_i} = 1$, where $\Gamma(\cdot)$ is the gamma function. It is shown in [33] that the generalized SNR distribution (5) can accurately represent all existing fading/shadowing channels, diversity-combining techniques and cooperative spectrum-sensing networks.

III. Performance Analysis at a Low SNR

This section, by using (5), develops a unified analysis for the low-SNR regime: i) average missed-detection probability; and ii) average AUC. Diversity combining and cooperative spectrum sensing are also investigated subsequently.

A. Average Missed-Detection Probability

Given the AWGN expression (4), average missed-detection probability over fading channels, $\overline{P_{\text{md}}}$, can be calculated by directly averaging over the SNR distribution to yield $\overline{P_{\text{md}}} = \int_0^\infty P_{\text{md}}(x) f_\gamma(x) dx$. Next we present a unified approach for this average, encompassing many existing fading channels, diversity-combining techniques, and cooperative sensing.

With the aid of (4), (5), $\text{Erfc}(-x) = 2 - \text{Erfc}(x)$, and some straightforward algebraic manipulations, average missed-detection probability over the generalized SNR distribution (5), denoted $\overline{P_{\text{md}}^{\text{Gen}}}$, can be given as

$$\overline{P_{\text{md}}^{\text{Gen}}} \approx \frac{1}{2}\sum_{i=1}^{S} \alpha_i \int_0^\infty x^{\beta_i - 1} e^{-\zeta_i x} \text{Erfc}\left(\sqrt{\frac{N}{2}}x + \frac{N\sigma_w^2 - \lambda}{\sqrt{2N}\sigma_w^2}\right) dx.$$

We now define an integral expression, $\mathcal{I}(n, p, c, d)$, which will be used in subsequent analysis, as [34, eq. (2.8.9.1)]

$$\mathcal{I}(n, p, c, d) \triangleq \int_0^\infty x^n e^{-px} \text{Erfc}(cx + d) dx = (-1)^n \frac{\partial^n \psi(p)}{\partial p^n}, \tag{6}$$

where

$$\psi(p) = \left[\frac{\text{Erfc}(d) - e^{\frac{p^2 + 4pcd}{4c^2}} \text{Erfc}\left(d + \frac{p}{2c}\right)}{p}\right],$$

n is a positive integer, Re[p]> 0, $c > 0, d > 0$, and $\frac{\partial^n}{\partial p^n}$ is the nth-order partial derivative with respect to p. Therefore, $\overline{P_{\text{md}}^{\text{Gen}}}$ can be derived for integer β_i as

$$\overline{P_{\text{md}}^{\text{Gen}}} \approx \frac{1}{2}\sum_{i=1}^{S} \alpha_i \mathcal{I}\left(\beta_i - 1, \zeta_i, \sqrt{\frac{N}{2}}, \frac{N\sigma_w^2 - \lambda}{\sqrt{2N}\sigma_w^2}\right). \tag{7}$$

This novel closed-form expression has a low computational complexity because of the following reasons.

In (7), we need $(\beta_i - 1)$th partial derivative (with respect to p) of $\psi(p)$ with

$$c = \sqrt{\frac{N}{2}}, \quad d = \frac{N\sigma_w^2 - \lambda}{\sqrt{2N}\sigma_w^2},$$

and β_i can take values $\beta_1, \cdots, \beta_S$. For fading channels, diversity or cooperative networks, β_i value may be a fading parameter, the number of diversity branches, or the number of cooperative nodes, which are small integer values. Further, values of β_i and S are typically small. Since $\psi(p)$ includes only exponential and $\text{Erfc}(\cdot)$ functions of p, its derivatives are also closed-form expressions for given β_i and S, including only exponential and $\text{Erfc}(\cdot)$ functions of p. The particular expressions are omitted for brevity. The most important fact is that the computational complexity of (7) does not increase with N (noting that the value of N is typically several thousands in the low-SNR regime). In contrast to (7), the complexity of other existing $\overline{P_d}$ expressions in the literature increases with N, for example:

- Confluent Hypergeometric functions and Laguerre polynomials [6], and generalized Hypergeometric functions [7] need infinite number of steps.
- The order of derivative equals the number of samples N for residue calculations, and subsequently infinite series are used in the calculation [8], or infinite-order derivatives are required [22].

Therefore, (7) is especially suited for the low-SNR regime, e.g., as used in the threshold selection analysis in Section IV.

Now we consider special cases of (7). For Rayleigh fading, the parameters are $S = 1$, $\alpha_1 = 1/\bar{\gamma}$ ($\bar{\gamma}$ is average SNR),

This article has been accepted for publication in a future issue of this journal, but has not been fully edited. Content may change prior to final publication. Citation information: DOI 10.1109/TVT.2014.2381648, IEEE Transactions on Vehicular Technology

$\beta_1 = 1$, and $\zeta_1 = 1/\bar{\gamma}$. Then the average missed-detection probability $\overline{P_{\text{md}}^{\text{Ray}}}$ is given as

$$\overline{P_{\text{md}}^{\text{Ray}}} \approx \frac{1}{2}\left[\text{Erfc}\left(\frac{N\sigma_w^2-\lambda}{\sqrt{2N}\sigma_w^2}\right) - e^{\frac{\frac{1}{\bar{\gamma}^2}+\frac{4}{\bar{\gamma}}\left(\frac{N\sigma_w^2-\lambda}{\sqrt{2N}\sigma_w^2}\right)\sqrt{\frac{N}{2}}}{2N}} \times \text{Erfc}\left(\frac{N\sigma_w^2-\lambda}{\sqrt{2N}\sigma_w^2}+\frac{1}{\bar{\gamma}\sqrt{2N}}\right)\right]. \quad (8)$$

For a Nakagami-m fading channel, the parameters are

$$S = 1,\ \alpha_1 = \frac{m^m}{\Gamma(m)\bar{\gamma}^m},\ \beta_1 = m,\ \zeta_1 = \frac{m}{\bar{\gamma}},$$

and the missed-detection probability, $\overline{P_{\text{md}}^{\text{Nak}}}$, is

$$\overline{P_{\text{md}}^{\text{Nak}}} \approx \frac{1}{2\Gamma(m)}\left(\frac{m}{\bar{\gamma}}\right)^m \mathcal{I}\left(m-1, \frac{m}{\bar{\gamma}}, \sqrt{\frac{N}{2}}, \frac{N\sigma_w^2-\lambda}{\sqrt{2N}\sigma_w^2}\right). \quad (9)$$

Similarly, the average missed-detection probabilities over many other existing fading channels (not only multipath fading channels) such as Nakagami-lognormal, K, K_G, η-μ, Nakagami-q (Hoyt), κ-μ, or Nakagami-n (Rician) can be derived easily after properly selecting the parameters S, α_i, β_i, ζ_i ($i = 1, 2, ..., S$).

For the square-law combining (SLC) with a low SNR, the false alarm probability and the missed-detection probability under AWGN channels can be evaluated as (3) and (4), respectively, with N replaced by LN (here L is the number of diversity branches). For fading channels, denote the SNR over the branches as $\gamma_1, \gamma_2, ..., \gamma_L$. If the PDF of $\gamma = \left[\sum_{i=1}^{L}\gamma_i\right]/L$ is modeled by using the generalized channel (5),[1] with the aid of (7), the average missed-detection probability can be derived as

$$\overline{P_{\text{md}}^{\text{Gen,SLC}}} \approx \frac{1}{2}\sum_{i=1}^{S}\alpha_i \mathcal{I}\left(\beta_i - 1, \zeta_i, \sqrt{\frac{LN}{2}}, \frac{LN\sigma_w^2-\lambda}{\sqrt{2LN}\sigma_w^2}\right). \quad (10)$$

Thus, the average missed-detection probability over a Rayleigh fading channel can be derived by using (10) with $S = 1$,

$$\alpha_1 = \frac{1}{\Gamma(L)}\left(\frac{L}{\bar{\gamma}}\right)^L,$$

$\beta_1 = L$ and $\zeta_1 = L/\bar{\gamma}$. Similarly, the average missed-detection probability over a Nakagami-m fading channel can be derived by using (10) with $S = 1$,

$$\alpha_1 = \frac{1}{\Gamma(mL)}\left(\frac{mL}{\bar{\gamma}}\right)^{mL},$$

$\beta_1 = mL$ and $\zeta_1 = mL/\bar{\gamma}$.

[1]As special cases, the PDF of $\gamma = \left[\sum_{i=1}^{L}\gamma_i\right]/L$ when signals of the branches follow i.i.d. Rayleigh and Nakagami-m fading are

$$f_\gamma(x) = \frac{1}{\Gamma(L)}\left(\frac{L}{\bar{\gamma}}\right)^L x^{L-1}e^{-\frac{L}{\bar{\gamma}}x},$$

$$f_\gamma(x) = \frac{1}{\Gamma(mL)}\left(\frac{mL}{\bar{\gamma}}\right)^{mL} x^{mL-1}e^{-\frac{mL}{\bar{\gamma}}x},$$

respectively, where $\bar{\gamma}$ is the average SNR at each branch [6].

If there are K cooperative nodes, each of which sends to a fusion center its own decision on presence/absence of the primary signal, and the fusion center uses the k-out-of-K fusion rule, the false alarm probability P_f^{Coop} and detection probability P_d^{Coop} at the fusion center can be written as

$$P_\chi^{\text{Coop}} = \sum_{i=k}^{K}\binom{K}{i}(p_\chi)^i(1-p_\chi)^{K-i},$$

where the notation 'χ' means 'f' for false alarm and means 'd' for detection. Here, the channels from the primary user to the cooperative nodes are assumed to be i.i.d., and thus, all the cooperative nodes can achieve identical false alarm probability p_f and detection probability p_d. Thus, the average missed-detection probability of cooperative spectrum sensing is

$$\overline{P_{\text{md}}^{\text{Gen,Coop}}} \approx 1 - \sum_{i=k}^{K}\binom{K}{i}\left(\overline{P_{\text{md}}^{\text{Gen}}}\right)^{K-i}\left(1-\overline{P_{\text{md}}^{\text{Gen}}}\right)^i, \quad (11)$$

with $\overline{P_{\text{md}}^{\text{Gen}}}$ given in (7).

B. Average Area under ROC Curve (AUC)

The ROC curve is the plot of P_d versus P_f as threshold λ varies from 0 to ∞. By eliminating the variable λ, P_d can be expressed as function of P_f. The area under the ROC curve is the AUC, which varies between 0.5 and 1. It represents the probability that the detector is more likely to choose the correct decision than the incorrect decision [35]. In Theorem 1, we derive a general expression for the AUC for AWGN channels.

Theorem 1. *Define*

$$P_f(\lambda) = \frac{1}{2}Erfc\left(\frac{\lambda-m_0}{\sqrt{2}\sigma_0}\right),\ P_d(\lambda) = \frac{1}{2}Erfc\left(\frac{\lambda-m_1}{\sqrt{2}\sigma_1}\right),$$

which are functions of λ ($-\infty < \lambda < \infty$),[2] where m_0, m_1, σ_0, and σ_1 are real positive values such that $m_0 \le m_1$ and $\sigma_0 \le \sigma_1$. By eliminating term λ, the two functions can be combined as

$$P_d = \frac{1}{2}Erfc\left(\frac{\sigma_0}{\sigma_1}Erfc^{-1}(2P_f) - \frac{m_1-m_0}{\sqrt{2}\sigma_1}\right),$$

which represents the P_d versus P_f curve. Thus, the area under the P_d versus P_f curve, $\mathcal{A}$, is given as

$$\mathcal{A} = 1 - \frac{1}{2}Erfc\left(\frac{m_1-m_0}{\sqrt{2(\sigma_0^2+\sigma_1^2)}}\right). \quad (12)$$

Proof: See Appendix A. ■

The instantaneous AUC of an energy detector at a low SNR can be derived from (12) by replacing $m_0 = N\sigma_w^2$, $m_1 = N\sigma_w^2(1+\gamma)$, $\sigma_0^2 = N\sigma_w^4$, and $\sigma_1^2 = N\sigma_w^4$, as

$$\mathcal{A}(\gamma) \approx 1 - \frac{1}{2}\text{Erfc}\left(\frac{\sqrt{N}}{2}\gamma\right).$$

[2]This is the theoretical limit of λ. But negative values of the threshold λ are not considered in practice.

This article has been accepted for publication in a future issue of this journal, but has not been fully edited. Content may change prior to final publication. Citation information: DOI 10.1109/TVT.2014.2381648, IEEE Transactions on Vehicular Technology

Now we derive the average AUC over the generalized SNR distribution (5) as $\overline{\mathcal{A}^{\text{Gen}}} = \int_0^\infty \mathcal{A}(x) f_\gamma(x) dx$, to yield

$$\begin{aligned}\overline{\mathcal{A}^{\text{Gen}}} &\approx 1 - \frac{1}{2}\sum_{i=1}^{S} \alpha_i \int_0^\infty x^{\beta_i - 1} e^{-\zeta_i x} \text{Erfc}\left(\frac{\sqrt{N}}{2} x\right) dx \\ &= 1 + \frac{1}{2}\sum_{i=1}^{S} (-1)^{\beta_i - 1} \alpha_i \\ &\quad \times \frac{\partial^{\beta_i - 1}}{\partial p^{\beta_i - 1}} \left(\frac{1}{p} e^{\frac{p^2}{N}} \text{Erfc}\left(\frac{p}{\sqrt{N}}\right) - \frac{1}{p}\right)\Bigg|_{p=\zeta_i},\end{aligned} \tag{13}$$

where β_i is a positive integer, and the equality in the second line of (13) comes after applying [34, eq. (2.8.5.4)]. This approximation can be used for many wireless channel models. For example, the average AUC over a Rayleigh fading channel, $\overline{\mathcal{A}^{\text{Ray}}}$, is

$$\overline{\mathcal{A}^{\text{Ray}}} \approx \frac{1}{2} + \frac{e^{\frac{1}{N\bar{\gamma}^2}}}{2} \text{Erfc}\left(\frac{1}{\bar{\gamma}}\sqrt{\frac{1}{N}}\right), \tag{14}$$

and the average AUC over a Nakagami-m fading channel, $\overline{\mathcal{A}^{\text{Nak}}}$, is

$$\begin{aligned}\overline{\mathcal{A}^{\text{Nak}}} &\approx 1 + \frac{(-1)^{m-1} m^m}{2\Gamma(m)\bar{\gamma}^m} \\ &\quad \times \frac{\partial^{m-1}}{\partial p^{m-1}} \left(\frac{1}{p} e^{\frac{p^2}{N}} \text{Erfc}\left(\frac{p}{\sqrt{N}}\right) - \frac{1}{p}\right)\Bigg|_{p=\frac{m}{\bar{\gamma}}},\end{aligned} \tag{15}$$

where m is an integer.

Similarly, for the SLC technique, the AUC over Nakagami-m fading channels can be derived by using (13) with

$$S = 1,\ \alpha_1 = \frac{1}{\Gamma(mL)} \left(\frac{mL}{\bar{\gamma}}\right)^{mL},\ \beta_1 = mL,\ \zeta_1 = \frac{mL}{\bar{\gamma}},$$

and with N replaced by LN. For cooperative spectrum sensing, because P_d^{Coop} is not expressible in terms of P_f^{Coop}, the AUC can be expressed as an integral only, which can be evaluated by numerical methods. However, a closed-form expression appears intractable.

IV. Threshold Selection

Threshold selection is traditionally based on the false alarm probability only, which, unfortunately, does not work for cognitive radio networks where missed-detection results in interference on primary users. While threshold selection with different objective functions (by relaxing some constraints) has been performed in [28], [29] and many others, these papers focus on non-fading scenarios, or do not consider both $P_{\text{md}}(\lambda)$ and $P_f(\lambda)$ simultaneously.

For a cognitive radio network, $P_{\text{md}}(\lambda)$ and $P_f(\lambda)$ must be below the thresholds denoted $P_{\text{md}}^{\text{th}}$ and P_f^{th}. Since $P_{\text{md}}(\lambda)$ increases and $P_f(\lambda)$ decreases with threshold λ, these requirements are equivalent to $\lambda \le \lambda_{\text{md}}^*$ and $\lambda \ge \lambda_f^*$ where $P_{\text{md}}(\lambda_{\text{md}}^*) = P_{\text{md}}^{\text{th}}$ and $P_f(\lambda_f^*) = P_f^{\text{th}}$.

If $\lambda_f^* > \lambda_{\text{md}}^*$, then there is no feasible λ that satisfies both false-alarm and missed-detection requirements, which necessitates other remedial actions, such as increasing the sampling rate. If $\lambda_f^* \le \lambda_{\text{md}}^*$, any λ value within range $[\lambda_f^*, \lambda_{\text{md}}^*]$ can satisfy both false-alarm and missed-detection constraints. In this range, optimal λ is then selected by optimizing a combination metric of both $P_f(\lambda)$ and $P_{\text{md}}(\lambda)$. For this purpose, the Bayesian cost [36], a popular metric to select the detection threshold [37]–[41], can be used. Minimizing the Bayesian cost is equivalent to minimizing the total error rate $P_e(\lambda) \triangleq P_f(\lambda) + P_{\text{md}}(\lambda)$. Therefore, the threshold selection problem is formulated as

$$\begin{aligned} \underset{\lambda}{\text{minimize}} \quad & P_e(\lambda) = P_f(\lambda) + P_{\text{md}}(\lambda) \\ \text{subject to} \quad & P_f(\lambda) \le P_f^{\text{th}} \\ & P_{\text{md}}(\lambda) \le P_{\text{md}}^{\text{th}}. \end{aligned} \tag{16}$$

We first relax the two constraints in (16), and denote the optimal solution as λ_e^*. Then the optimal solution for problem (16), denoted λ^*, is given as

$$\lambda^* = \begin{cases} \lambda_e^* : \text{ if } \lambda_f^* \le \lambda_{\text{md}}^* \text{ and } \lambda_e^* \in [\lambda_f^*, \lambda_{\text{md}}^*], \\ \lambda_f^* \text{ or } \lambda_{\text{md}}^*, \text{ whichever is closer to } \lambda_e^* : \text{ if } \lambda_f^* \le \lambda_{\text{md}}^* \\ \qquad\qquad \text{and } \lambda_e^* \notin [\lambda_f^*, \lambda_{\text{md}}^*], \\ \text{no solution : if } \lambda_f^* > \lambda_{\text{md}}^*. \end{cases}$$

Since $P_f(\lambda)$ does not depend on fading effect, λ_f^* can be derived regardless of any fading scenario by using (3) as

$$\lambda_f^* = \left(\sqrt{\frac{2}{N}} \text{Erfc}^{-1}\left(2P_f^{\text{th}}\right) + 1\right) N\sigma_w^2. \tag{17}$$

In the following, we derive exact λ_{md}^* and λ_e^* for AWGN channels and approximate them for multipath fading channels. Generally, for any fading model (Gaussian, Rayleigh, etc.), minimum $P_e(\lambda)$ is achieved when $\frac{\partial P_e(\lambda)}{\partial \lambda} = 0$, which is illustrated in Appendix B.

A. AWGN Channel

In this case, rather than using the low-SNR model in (2), we consider the general SNR case in (1), which leads to closed-form expressions of λ_{md}^* and λ_e^*, as follows.[3] For **S1** or **S3** signal model with any SNR value γ, λ_{md}^* can be derived by using (1) as

$$\lambda_{\text{md}}^* = \left(\sqrt{\frac{2(1+2\gamma)}{N}} \text{Erfc}^{-1}\left(2(1 - P_{\text{md}}^{\text{th}})\right) + (1+\gamma)\right) N\sigma_w^2, \tag{18}$$

and λ_e^* is given by using (1) as

$$\begin{aligned}\lambda_e^* &= \arg\min_{\lambda} \left(1 + \frac{1}{2}\text{Erfc}\left(\frac{\lambda - N\sigma_w^2}{\sqrt{2N}\sigma_w^2}\right)\right. \\ &\qquad \left. - \frac{1}{2}\text{Erfc}\left(\frac{\lambda - N\sigma_w^2(1+\gamma)}{\sqrt{2N(1+2\gamma)}\sigma_w^2}\right)\right) \\ &= \frac{N\sigma_w^2}{2}\left(1 + \sqrt{1 + 2\gamma\left(1 + \frac{(1+2\gamma)\ln(1+2\gamma)}{N\gamma^2}\right)}\right),\end{aligned} \tag{19}$$

[3]This implies that the derived (18), (19), and (20) are valid from low to high SNR.

This article has been accepted for publication in a future issue of this journal, but has not been fully edited. Content may change prior to final publication. Citation information: DOI 10.1109/TVT.2014.2381648, IEEE Transactions on Vehicular Technology

where the second equality comes as explained in Appendix C. Similarly, λ^*_{md} and λ^*_e for **S2** signal model can be derived as

$$\lambda^*_{\text{md}} = \left(\sqrt{\frac{2}{N}}(1+\gamma)\text{Erfc}^{-1}\left(2(1-P^{\text{th}}_{\text{md}})\right) + (1+\gamma)\right)N\sigma_w^2,$$
$$\lambda^*_e = \frac{N\sigma_w^2}{2}\left(1+\sqrt{1+\frac{2(2+\gamma)\ln(1+\gamma)}{N\gamma}}\right)\left(\frac{1+\gamma}{1+\frac{\gamma}{2}}\right). \quad (20)$$

B. Multipath Fading

In Rayleigh and Nakagami-m fading in the low-SNR regime, the exact closed-form λ^*_{md} and λ^*_e are intractable from missed-detection probabilities (8) and (9), although numerical computation is feasible. As a result, we derive approximations for Rayleigh and Nakagami-2 fading channels. Our procedure can also be extended for arbitrary $m \geq 2$. The approximations and simulations are compared in Table II in Section V, showing a close match.

1) Rayleigh Fading Channel: We define

$$\alpha \triangleq \frac{N\sigma_w^2 - \lambda}{\sqrt{2N}\sigma_w^2},\ a \triangleq \frac{1}{\sqrt{2N\bar{\gamma}}},$$

which will be used in this section. By using (8), $\overline{P^{\text{Ray}}_{\text{md}}}(\lambda)$ can be written as

$$\overline{P^{\text{Ray}}_{\text{md}}}(\lambda) \approx \frac{1}{2}\Big[\text{Erfc}\,(\alpha) - e^{a^2}e^{2a\alpha}\text{Erfc}\,(a+\alpha)\Big]. \quad (21)$$

Thus, an approximate λ^*_{md} can be calculated as (22) on the next page, where $u = ae^{a^2}\text{Erfc}(a)$. The derivation is given in Appendix D1.

The total error rate is $P_e(\lambda) = P_f(\lambda) + \overline{P^{\text{Ray}}_{\text{md}}}(\lambda)$. For minimum $P_e(\lambda)$, an approximate threshold can be given as

$$\lambda^*_e \approx \left(1 + \frac{1}{N\bar{\gamma}} - \sqrt{\frac{2}{N\pi}} + \sqrt{\frac{2}{N}\left(\frac{1}{\pi} + \sqrt{\frac{2N}{\pi}}\bar{\gamma} - 1\right)}\right)N\sigma_w^2. \quad (23)$$

The derivation is given in Appendix D2.

2) Nakagami-2 Fading Channel: By using (9), $\overline{P^{\text{Nak}}_{\text{md}}}(\lambda)$ for Nakagami-2 fading channel can be written as

$$\overline{P^{\text{Nak}}_{\text{md}}}(\lambda) \approx \frac{1}{2}\text{Erfc}(\alpha) - \frac{2a}{\sqrt{\pi}}e^{-\alpha^2} + \left(4a^2 - \frac{1}{2} + 2a\alpha\right)e^{4a^2}e^{4a\alpha}\text{Erfc}(2a+\alpha). \quad (24)$$

Thus, λ^*_{md} can be calculated as (25) on next page, where $v = a^2e^{4a^2}\text{Erfc}(2a)$. The derivation is given in Appendix E1.

The total error rate is $P_e(\lambda) = P_f(\lambda) + \overline{P^{\text{Nak}}_{\text{md}}}(\lambda)$. For minimum $P_e(\lambda)$, an approximate threshold can be given as

$$\lambda^*_e \approx \left[1 + \frac{2}{N\bar{\gamma}} - \frac{1}{2\sqrt{2N}}\left(\sqrt{\pi} - \sqrt{\pi - 8 + 2N\bar{\gamma}^2}\right)\right]N\sigma_w^2. \quad (26)$$

The derivation is given in Appendix E2.

3) Nakagami-m Fading Channel: For a given fading parameter m, $\overline{P^{\text{Nak}}_{\text{md}}}$ can be derived in closed-form by using (9), which includes only exponential and Erfc$(\cdot)$ functions. Following the similar procedure given in Section IV-B2, approximate λ^*_{md} and λ^*_e for a general Nakagami-m fading channel can easily be derived analytically. Moreover, by keeping increasing the number of terms of Taylor series expansions (e.g., polynomial with degree greater than 2), we can find more accurate approximations for λ^*_{md} and λ^*_e.

C. Diversity Combining or Cooperative Spectrum Sensing

If SLC is used, the results in Section IV-A can be applied with N replaced by LN for SLC over AWGN in which $\gamma = \left[\sum_{i=1}^{L}\gamma_i\right]/L$, and numerical methods can be used for other fading channels by using (10). Similarly, if cooperative sensing is used, the optimal threshold can be determined by numerical methods by using (11).

V. Numerical/Simulation Results and Discussion

This section provides numerical results based on our preceding analysis, and semi-analytical Monte-Carlo simulation results based on the system model in Section II. Because all signal models perform more or less the same at low SNR, simulation is limited to **S1** signal model only.

The *normalized threshold* is defined as $\hat{\lambda} \triangleq \lambda/N$.[4] The noise variance is set to $\sigma_w^2 = 1$. For SLC and cooperative spectrum sensing, only Rayleigh fading is considered. The Rayleigh fading case provides a worst-case benchmark because its performance is much worse than those of AWGN and Nakagami-m ($m > 1$) fading channels.

A. Accuracy of our low-SNR missed-detection probability expressions

The ROC curves are calculated from (4), (8)-(11), and simulated (Figs. 1 and 2). Specifically, Fig. 1 shows the ROC curves for AWGN, Rayleigh and Nakagami-4 fading channels with -20 dB average SNR. The ROC curves are plotted in the range $\hat{\lambda} \in [0.95, 1.05]$ and $\hat{\lambda} \in [0.995, 1.02]$ for $N = 2\times10^3$ and $N = 2\times10^5$, respectively. Fig. 2 shows the ROC curves of SLC with $L = 2, 3$ and cooperative spectrum sensing (with *OR* decision fusion rule) with $K = 2, 3$ over Rayleigh fading at $\bar{\gamma}$= -20 dB when N takes two values: when $N = 2\times10^3$, the ROC curves are plotted in the range $\hat{\lambda} \in [1.92, 2.10]$ and $\hat{\lambda} \in [2.94, 3.10]$ for SLC with $L = 2$ and 3, respectively, and in the range $\hat{\lambda} \in [0.95, 1.1]$ for cooperative spectrum sensing; when $N = 2\times10^6$, the ROC curves are plotted in the range $\hat{\lambda} \in [2.00, 2.02]$ and $\hat{\lambda} \in [3.00, 3.03]$ for SLC with $L = 2$ and 3, respectively, and in the range $\hat{\lambda} \in [0.99, 1.03]$ for cooperative spectrum sensing. The analytical results perfectly match the simulation results for a high and low number of samples, and also for high and low P_d and P_f, confirming the accuracy of our low-SNR approximations in (4), (8)-(11). These figures show that when $N = 2\times10^3$, the IEEE 802.22 requirements on false alarm and missed-detection probabilities

[4]This is the threshold if the decision statistic is selected as $\Lambda = \left[\sum_{n=1}^{N}|y(n)|^2\right]/N$.

This article has been accepted for publication in a future issue of this journal, but has not been fully edited. Content may change prior to final publication. Citation information: DOI 10.1109/TVT.2014.2381648, IEEE Transactions on Vehicular Technology

$$\lambda^*_{\text{md}} \approx \left[1 - \sqrt{\frac{2}{N}}\left(\frac{\sqrt{\pi}u - \pi^{1/4}\sqrt{4P^{\text{th}}_{\text{md}}a - 2a - u\left(2a(2P^{\text{th}}_{\text{md}}-1)\sqrt{\pi}+\sqrt{\pi}u-2\right)}}{2a(1-\sqrt{\pi}u)}\right)\right] N\sigma_w^2 \tag{22}$$

$$\lambda^*_{\text{md}} \approx \left[1 - \frac{\left(4a^2 - 8\sqrt{\pi}av - \sqrt{2}\sqrt{\left(\pi v\left(\left(2P^{\text{th}}_{\text{md}}-1\right)\left(1+8a^2\right) - \left(32a^2 - a^{-2}\right)v\right) - 8a^4 + 4\sqrt{\pi}a^2\left(a - 2P^{\text{th}}_{\text{md}}a + 8av\right)\right)}\right)\bar{\gamma}}{4\left(\sqrt{\pi}\left(1+8a^2\right)v - 4a^3\right)}\right] N\sigma_w^2 \tag{25}$$

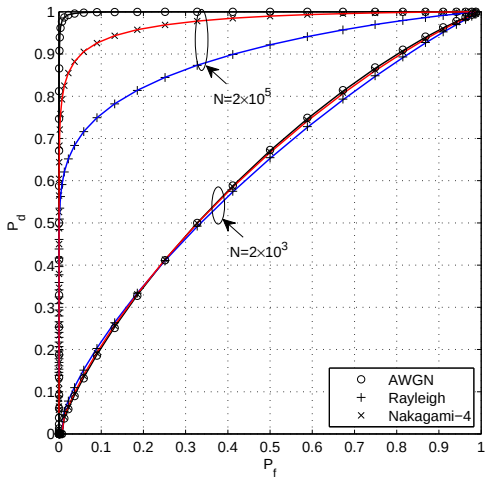

Fig. 1: Approximate (low-SNR analysis) ROC curves (solid lines) and simulated ROC curves (discrete marks) of AWGN, Rayleigh and Nakagami-4 fading channels for $N = 2 \times 10^3$ and $N = 2 \times 10^5$ at -20 dB SNR.

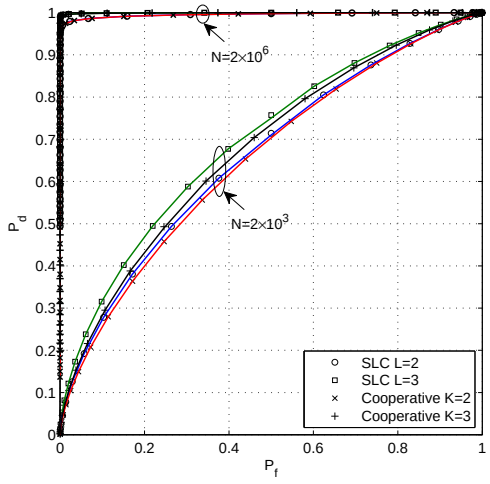

Fig. 2: Approximate (low-SNR analysis) ROC curves (solid lines) and simulated ROC curves (discrete marks) of SLC when $L = 2, 3$ and cooperative spectrum sensing when $K = 2, 3$ for $N = 2 \times 10^3$ and $N = 2 \times 10^6$ over Rayleigh fading at -20 dB SNR.

cannot be satisfied simultaneously in any case in the two figures; when $N = 2 \times 10^5$, the requirements can be satisfied simultaneously for all cases in Fig. 1 except Rayleigh fading case; when $N = 2 \times 10^6$, the requirements can be satisfied simultaneously for all cases in Fig. 2. Thus, the impact of using more samples, more diversity branches or more cooperative nodes is clearly positive.

B. Low-SNR AUC approximations

By using eqs. (14) and (15), Table I lists results for three channels and SLC. Our approximations match closely with the simulations. As expected, AUCs for AWGN and Rayleigh cases vary from the largest to the smallest. With SLC, a larger number of branches leads to a higher AUC and provides better overall detection capability. Obviously, a larger number of samples also leads to a higher AUC confirming a better overall detection capability.

C. Threshold selection

The optimal threshold, λ^*, is determined by minimizing the total error rate as in (16). We denote $P_e^* = P_e(\lambda^*)$, $P_f^* = P_f(\lambda^*)$, and $P^*_{\text{md}} = \overline{P_{\text{md}}}(\lambda^*)$. When $\bar{\gamma} = -20$ dB and $N = 2 \times 10^6$, Fig. 3 and Fig. 4 show low-SNR approximate total error rates (analytical results represented by solid lines, where the average missed-detection probability is calculated based on our analysis in Section III-A) and simulated total error rates (represented by discrete marks) versus the normalized threshold for the AWGN, Rayleigh, Nakagami-2 fading channels, cooperative spectrum sensing ($K = 2$), and SLC diversity combining ($L = 3$). Since the analytical results perfectly match the simulation results in Figs. 3 and 4, Table II shows only the numerically calculated normalized threshold values ($\hat{\lambda}_f^*$, $\hat{\lambda}^*_{\text{md}}$, $\hat{\lambda}_e^*$, $\hat{\lambda}^*$) ($\hat{\lambda}_f^*$ and $\hat{\lambda}^*_{\text{md}}$ are calculated under constraints $P_f(\lambda) \leq 0.1$ and $\overline{P_{\text{md}}}(\lambda) \leq 0.1$, respectively), and numerically calculated false alarm probability, missed-detection probability, and total error rate at $\hat{\lambda}_e^*$. In Table II, the numbers in brackets are approximated $\hat{\lambda}^*_{\text{md}}$ and $\hat{\lambda}_e^*$ for Rayleigh fading channels based on (22) and (23) and for Nakagami-2 fading channels based on (25) and (26).[5] From Table II, we have $\hat{\lambda}_f^* < \hat{\lambda}_e^* < \hat{\lambda}^*_{\text{md}}$ for AWGN channel, Nakagami-2 channel, SLC diversity combining, and cooperative sensing, and thus, $\hat{\lambda}^* = \hat{\lambda}_e^*$. However, for Rayleigh

[5]For AWGN channels, we have exact analytical solution for $\hat{\lambda}^*_{\text{md}}$ and $\hat{\lambda}_e^*$ as given in (18) and (19). For SLC or cooperative sensing over fading channels, we do not have analytical results for $\hat{\lambda}^*_{\text{md}}$ and $\hat{\lambda}_e^*$.

This article has been accepted for publication in a future issue of this journal, but has not been fully edited. Content may change prior to final publication. Citation information: DOI 10.1109/TVT.2014.2381648, IEEE Transactions on Vehicular Technology

Fig. 1	$N = 2 \times 10^3$	$N = 2 \times 10^5$	Fig. 2	$N = 2 \times 10^3$	$N = 2 \times 10^6$
AWGN	0.624085 (0.623489)	0.999217 (0.999174)	SLC $L = 2$	0.663636 (0.662751)	0.995683 (0.995679)
Nakagami-4	0.622408 (0.62172)	0.974777 (0.97462)	SLC $L = 3$	0.698242 (0.697292)	0.999455 (0.999455)
Rayleigh	0.616163 (0.615361)	0.895188 (0.895034)			

TABLE I: AUC approximations and simulated values (in the brackets) for AWGN, Rayleigh, Nakagami-4 channels in Fig. 1 and SLC ($L = 2, 3$) in Fig. 2.

	AWGN	Rayleigh	Nakagami-2	SLC $L = 3$ over Rayleigh	Cooperative $K = 2$ over Rayleigh
$\hat{\lambda}_f^*$	1.00091	1.00091	1.00091	3.00157	1.00116
$\hat{\lambda}_{\text{md}}^*$	1.00908	1.00106 (1.0010)	1.00261 (1.00291)	3.01096	1.00383
$\hat{\lambda}_e^*$	1.00498	1.00138 (1.0027)	1.00160 (1.00463)	3.00357	1.00192
$P_f(\hat{\lambda}_e^*)$	9.90×10^{-13}	0.02	0.004	0.002	0.007
$P_{\text{md}}(\hat{\lambda}_e^*)$	9.90×10^{-13}	0.13	0.011	0.007	0.030
$P_e(\hat{\lambda}_e^*)$	1.98×10^{-12}	0.15	0.015	0.009	0.037
$\hat{\lambda}^*$	$\hat{\lambda}_e^*$	$\hat{\lambda}_{\text{md}}^*$	$\hat{\lambda}_e^*$	$\hat{\lambda}_e^*$	$\hat{\lambda}_e^*$

TABLE II: Normalized threshold values ($\hat{\lambda}_f^*$, $\hat{\lambda}_{\text{md}}^*$, $\hat{\lambda}_e^*$, $\hat{\lambda}^*$) and error probabilities (P_f, P_{md}, P_e) at $\hat{\lambda}_e^*$ for AWGN, Rayleigh and Nakagami-2 channels, SLC, and cooperative spectrum sensing when $N = 2 \times 10^6$ and $\bar{\gamma} = -20$ dB. The numbers in brackets are approximated $\hat{\lambda}_{\text{md}}^*$ and $\hat{\lambda}_e^*$ based on (22) and (23) for Rayleigh fading channels and based on (25) and (26) for Nakagami-2 fading channels, respectively. $\hat{\lambda}_f^*$ and $\hat{\lambda}_{\text{md}}^*$ are calculated under constraints $P_f(\lambda) \leq 0.1$ and $\overline{P_{\text{md}}}(\lambda) \leq 0.1$, respectively.

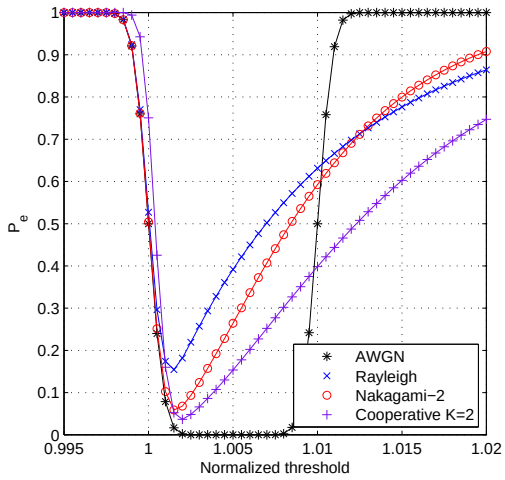

Fig. 3: Approximate total error rate (solid lines) and simulated total error rate (discrete marks) versus normalized threshold in AWGN, Rayleigh and Nakagami-2 channels and cooperative spectrum sensing ($K = 2$) over Rayleigh fading.

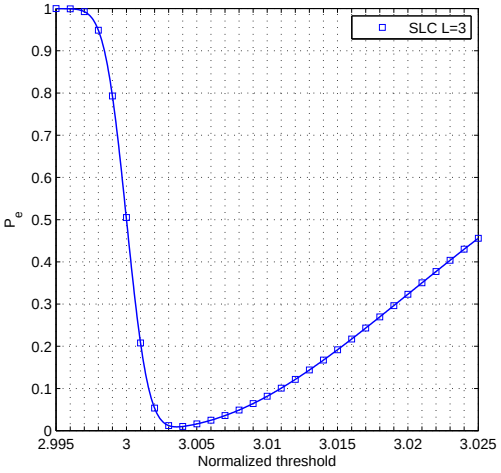

Fig. 4: Approximate total error rate (solid lines) and simulated total error rate (discrete marks) versus normalized threshold in SLC ($L = 3$) over Rayleigh fading, for $N = 2 \times 10^6$ at -20 dB average SNR.

channel, $\hat{\lambda}_f^* < \hat{\lambda}_{\text{md}}^* < \hat{\lambda}_e^*$, and thus, $\hat{\lambda}^* = \hat{\lambda}_{\text{md}}^*$.

Next we focus on the IEEE 802.22 requirements for spectrum sensing by using standard parameter values. These requirements specify that $P_f \leq 0.1$ and $\overline{P_{\text{md}}} \leq 0.1$, and that the channel sensing time $\tau \leq 2$ seconds. Since $N \approx \tau f_s$ where f_s is the sampling rate, which may depend on the sampling frequency of the analog-to-digital converter (ADC) and the FFT (fast Fourier transform) bin resolution, N cannot be increased beyond τf_s. In an experimental energy detection implementation [42], f_s is selected as $f_s = 62.5$ kHz which may be a typical test-bed FFT bin resolution for moderate or high SNR. However, f_s can take several mega-hertz in other typical system implementations, e.g., some advanced ADCs can operate at $f_s = 20$ MHz [43], 500 MHz [44], which may benefit low-SNR sensing. In our work, we limit $f_s = 1$ MHz, and thus the maximal value of N is 2×10^6 for 2 seconds of sensing time.[6]

Fig. 5, Fig. 6, and Fig. 7 show analytical error rates (represented by lines) and simulated error rates (represented by discrete marks) at the optimal threshold ($P_f^* = P_f(\lambda^*)$, $P_{\text{md}}^* = P_{\text{md}}(\lambda^*)$, and $P_e^* = P_e(\lambda^*)$) versus N for fading channels (AWGN, Rayleigh and Nakagami-4), diversity technique (SLC) and cooperative spectrum sensing with -20 dB average

[6]Since we only consider the sensing but not the subsequent processing, 2 seconds is used as a reference sensing time. For a fixed N, sensing time can be proportionally reduced by using a higher sampling rate, e.g., we can have 2×10^6 samples within 10 milliseconds at $f_s = 200$ MHz as in [45].

This article has been accepted for publication in a future issue of this journal, but has not been fully edited. Content may change prior to final publication. Citation information: DOI 10.1109/TVT.2014.2381648, IEEE Transactions on Vehicular Technology

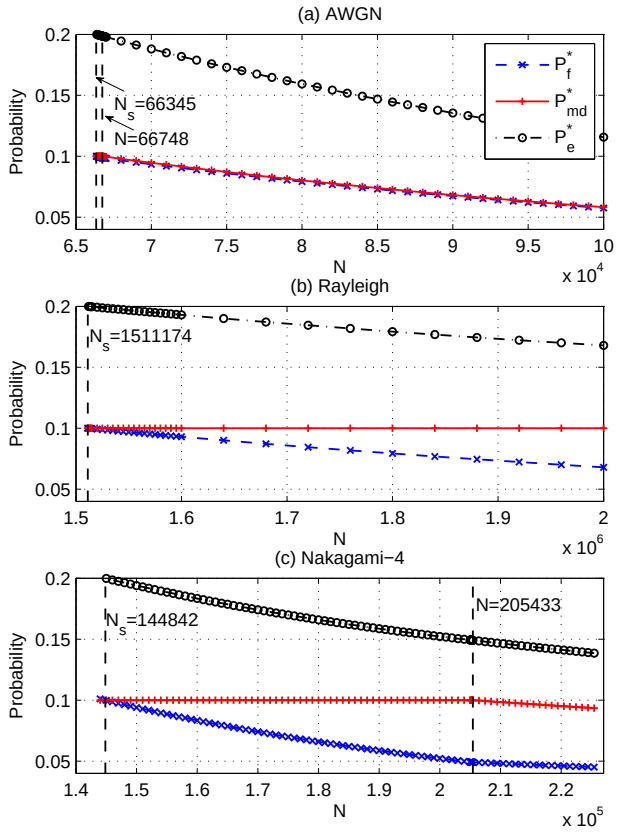

Fig. 5: Analytical error rates (lines) and simulated error rates (discrete marks) at the optimal threshold value (total error: P_e^*; false alarm: P_f^*; and missed-detection: P_{md}^*) versus the number, N, of samples at -20 dB average SNR for (a) AWGN; (b) Rayleigh; (c) Nakagami-4 fading channels.

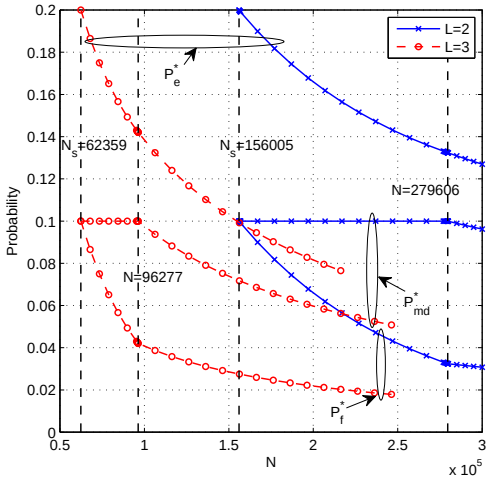

Fig. 6: Analytical error rates (lines) and simulated error rates (discrete marks) at the optimal threshold value (total error: P_e^*; false alarm: P_f^*; and missed-detection: P_{md}^*) versus the number, N, of samples at -20 dB average SNR for SLC when $L = 2, 3$.

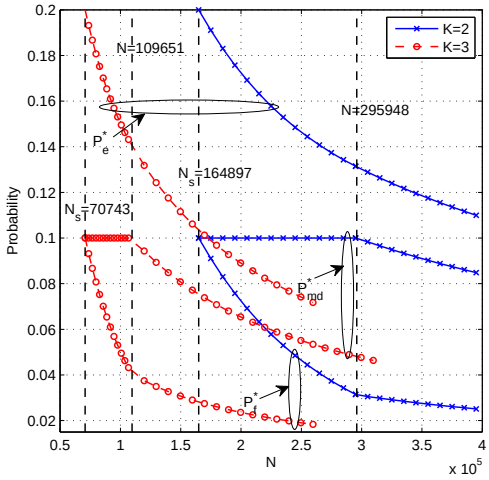

Fig. 7: Analytical error rates (lines) and simulated error rates (discrete marks) at the optimal threshold value (total error: P_e^*; false alarm: P_f^*; and missed-detection: P_{md}^*) versus the number, N, of samples at -20 dB average SNR for cooperative spectrum sensing when $K = 2, 3$, over Rayleigh fading.

SNR. The optimal threshold, λ^*, is calculated based on low-SNR analysis in Section IV. Recall that an optimal threshold can be found only when $\lambda_f^* \leq \lambda_{\text{md}}^*$, which is equivalent to $N \geq N_s$ where N_s is the minimum number of samples to have a feasible detection threshold that satisfies both requirements on false alarm and missed-detection probabilities. Under this condition ($N \geq N_s$), we may have three possible cases such as (i) $\lambda_f^* \leq \lambda_{\text{md}}^* \leq \lambda_e^*$; (ii) $\lambda_f^* \leq \lambda_e^* \leq \lambda_{\text{md}}^*$; or (iii) $\lambda_e^* \leq \lambda_f^* \leq \lambda_{\text{md}}^*$. As examples given in Fig. 5, Fig. 6, and Fig. 7, we do not have the third case.

Based on our analytical results in Fig. 5, Fig. 6, and Fig. 7, the regions of N for different possible cases are shown in Table III.[7] Table III also includes the minimal sensing time to have a feasible detection threshold when $f_s = 1$ MHz, given as $\tau_{\min} = N_s/(1\text{ MHz})$, and the minimal sampling rate to have a feasible detection threshold when the sensing time is 2 seconds, given as $f_{s,\min} = N_s/(2\text{ sec})$. We use two cases in Fig. 5: AWGN and Rayleigh fading cases, as examples. For the AWGN channel, there is no feasible detection threshold when $N < N_s = 66345$. When $N \in [66345, 66747]$, we have $\lambda_f^* \leq \lambda_{\text{md}}^* \leq \lambda_e^*$, the optimal threshold is determined by the missed-detection probability requirement, and thus, in this region of N, P_{md}^* keeps at 0.1, and P_f^* is slightly below 0.1. When $N \geq 66748$, we have $\lambda_f^* \leq \lambda_e^* \leq \lambda_{\text{md}}^*$, and the optimal threshold is determined by minimizing the total error rate. For Rayleigh fading channel, there is no feasible detection threshold when $N < N_s = 1511174$. When N varies from N_s to 2×10^6 (the maximal number of samples when $f_s = 1$ MHz and sensing time $\tau = 2$ seconds), we have $\lambda_f^* \leq \lambda_{\text{md}}^* \leq \lambda_e^*$, and the optimal threshold is determined by the missed-detection probability requirement, and thus, P_{md}^* keeps at 0.1

[7]Since analytical and simulation results in Fig. 5, Fig. 6, and Fig. 7 perfectly match, we only use the analytical results to generate Table III.

This article has been accepted for publication in a future issue of this journal, but has not been fully edited. Content may change prior to final publication. Citation information: DOI 10.1109/TVT.2014.2381648, IEEE Transactions on Vehicular Technology

	N				$\tau_{\min}$ (sec) at $f_s = 1$ MHz	$f_{s,\min}$ (kHz) at $\tau = 2$ sec
	$\lambda_f^* > \lambda_{\text{md}}^*$	$\lambda_f^* \le \lambda_{\text{md}}^* \le \lambda_e^*$	$\lambda_f^* \le \lambda_e^* \le \lambda_{\text{md}}^*$	$\lambda_e^* \le \lambda_f^* \le \lambda_{\text{md}}^*$		
AWGN	≤ 66344	$[66345, 66747]$	≥ 66748	–	0.07	33.2
Rayleigh	≤ 1511173	$[1511174, 3871892]$	≥ 3871893	–	1.51	755.6
Nakagami-4	≤ 144841	$[144842, 205432]$	≥ 205433	–	0.14	72.4
SLC $L = 2$	≤ 156004	$[156005, 279605]$	≥ 279606	–	0.16	78.0
SLC $L = 3$	≤ 62358	$[62359, 96276]$	≥ 96277	–	0.06	31.2
Cooperative $K = 2$	≤ 164896	$[164897, 295947]$	≥ 295948	–	0.16	82.4
Cooperative $K = 3$	≤ 70742	$[70743, 109650]$	≥ 109651	–	0.07	35.4

TABLE III: The regions of N for different cases of $\lambda_f^*, \lambda_{\text{md}}^*, \lambda_e^*$, the minimal sensing time $\tau_{\min}$ at $f_s = 1$ MHz, and the minimal sampling rate $f_{s,\min}$ at $\tau = 2$ seconds.

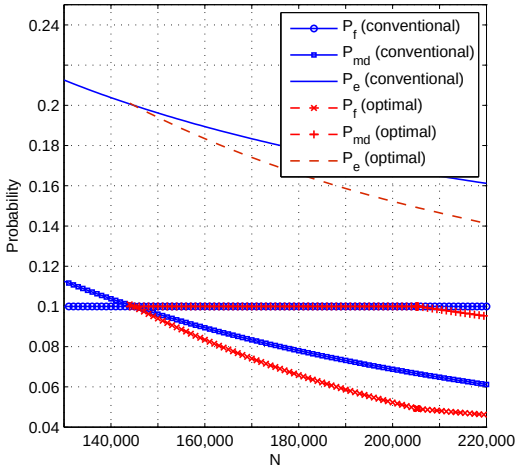

Fig. 8: Error rates versus the number of samples of conventional and optimal threshold selection methods over Nakagami-4 fading channels at -20 dB average SNR.

in this region of N.

In the following, we focus on diversity-combining (SLC with $L = 2, 3$) and cooperative spectrum sensing ($K = 2, 3$), which can be used to increase the effective number of samples in the decision statistic without increasing the sampling rate. The Rayleigh fading channel is considered to establish the worse case scenario. From Table III, for two or three diversity branches in SLC, N_s is reduced from N_s =1511174 (no diversity) to N_s =156005 or 62359, respectively, which results in the minimum sensing time at $f_s = 1$ MHz as $\tau_{\min} \approx$ 0.16 or 0.06 seconds, and the minimal sampling rate at $\tau = 2$ seconds as $f_{s,\min} \approx 78.0$ kHz or 31.2 kHz, respectively. Similarly, for two or three cooperative nodes in a cooperative spectrum sensing network with OR fusion rule, the minimum sensing time is $\tau_{\min} \approx 0.16$ or 0.07 seconds, and the minimal sampling rate is $f_{s,\min} \approx 82.4$ kHz or 35.4 kHz, respectively. Thus, to satisfy both IEEE 802.22 requirements on false alarm and missed-detection probabilities, diversity combining and cooperative spectrum sensing can significantly reduce the required sensing time and/or the required sampling rate.

In Fig. 8, simulation results are provided to compare our (optimal) threshold selection with a conventional threshold selection (calculated from $P_f = 0.1$). A Nakagami-4 fading channel with -20 dB SNR is considered. Note that conventional threshold selection does not guarantee a bounded missed-detection probability, which is evident from the figure. For example, when $N < 144842$, $P_{\text{md}} \le 0.1$ is not satisfied, and thus, excess interference to primary users can be generated. When $N \ge 144842$, the optimal and conventional threshold selection can keep both P_{md} and P_f bounded by 0.1. But our optimal scheme has a lower total error rate because P_f drops dramatically, improving spectral efficiency.

D. Discussion for Case with Noise Uncertainty

Following [46], it is well known that uncertainty of the noise power level can significantly degrade the spectrum sensing capability of the energy detector. This has given rise to the so-called SNR wall phenomenon. According to [46], noise uncertainty is modeled as $\sigma_w^2 \in \left[(1/\rho)\sigma_n^2,\ \rho\sigma_n^2\right]$ where σ_n^2 is the nominal noise power and $\rho \ge 1$. Thus, if we denote P_f and $\overline{P_{\text{md}}^{\text{Gen}}}$ in (3) and (7) as $P_{f|\sigma_w^2}$ and $\overline{P_{\text{md}|\sigma_w^2}^{\text{Gen}}}$, respectively, and denote the probability density function of $\sigma_w^2 \in \left[(1/\rho)\sigma_n^2,\ \rho\sigma_n^2\right]$ as $g_{\sigma_w^2}(\cdot)$, then the false alarm probability can be given as

$$P_f = \int_{(1/\rho)\sigma_n^2}^{\rho\sigma_n^2} P_{f|\sigma_w^2} g_{\sigma_w^2}(x)dx,$$

and the average missed-detection probability can be given as

$$\overline{P_{\text{md}}^{\text{Gen}}} = \int_{(1/\rho)\sigma_n^2}^{\rho\sigma_n^2} \overline{P_{\text{md}|\sigma_w^2}^{\text{Gen}}} g_{\sigma_w^2}(x)dx. \tag{27}$$

However, the analytical complexity depends on the nature of $g_{\sigma_w^2}(\cdot)$ expression, and it may not guarantee a closed-form and/or tractable expression for the threshold selection.

As an example, similar to [47], assume σ_w^2 to be a uniform random variable between $\left[(1/\rho)\sigma_n^2,\ \rho\sigma_n^2\right]$. Considering Nakagami-4 fading channel, we plot Fig. 9, based on (27) in which $\overline{P_{\text{md}|\sigma_w^2}^{\text{Gen}}}$ is given in (9), with $\sigma_n^2 = 1$ and $N = 2 \times 10^6$. Since larger ρ means higher uncertainty, we can readily see that the performance degrades rapidly with higher ρ.

VI. Conclusion

This paper analyzed the performance of energy detection in low SNR, deriving new missed-detection probability and AUC expressions. The criterion for optimal threshold was formulated to minimize the total error rate subject to bounded false alarm and miss-detection probabilities. Optimal thresholds were then derived for non-fading channels in closed-form and for multipath fading channels in approximate form. Diversity combining techniques and cooperative spectrum sensing were

This article has been accepted for publication in a future issue of this journal, but has not been fully edited. Content may change prior to final publication. Citation information: DOI 10.1109/TVT.2014.2381648, IEEE Transactions on Vehicular Technology

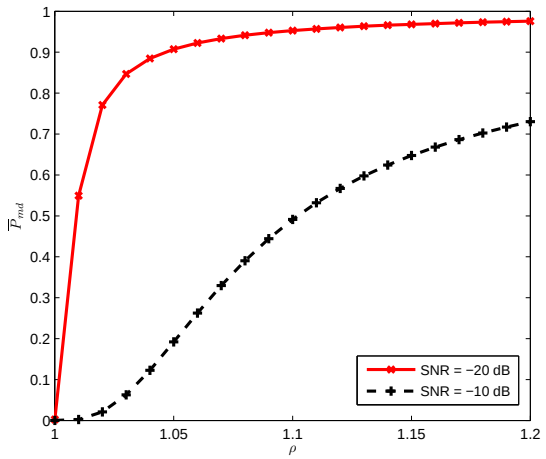

Fig. 9: Noise uncertainty: $\overline{P_{\text{md}}^{\text{Gen}}}$ versus ρ.

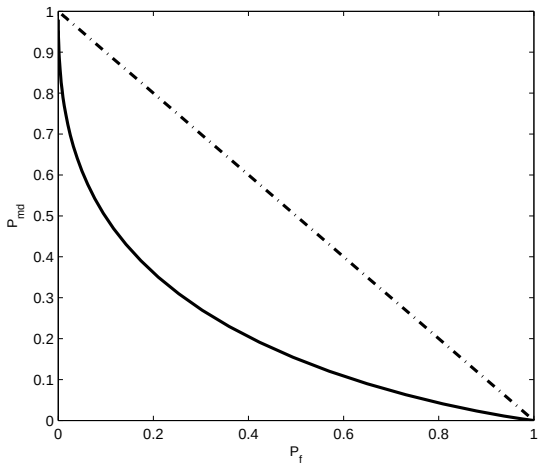

Fig. 10: An illustration of complementary ROC curve.

shown to reduce the needed sensing time or sampling rate, enabling low-SNR detection. Low-SNR detection can play a useful role in the emerging cognitive radio networks.

While this paper considered a single secondary user and one primary spectrum band, this setup can be extended to cases with multiple secondary users and multiple primary spectrum bands. In this context, our analytical framework can be used to derive the detection performance and/or to select the detection threshold for any secondary user over any spectrum band. If a traffic model is specified for the secondary users, interesting future research topics may include optimal resource allocation to maximize the secondary network throughput.

APPENDIX

A. Proof of Theorem 1

As λ varies from $-\infty$ to ∞, P_f varies from 1 to 0. Therefore, the area under P_d versus P_f curve can be written as

$$\begin{aligned}\mathcal{A} &= \int_0^1 \frac{1}{2}\text{Erfc}\left(\frac{\sigma_0}{\sigma_1}\text{Erfc}^{-1}(2x) - \frac{m_1-m_0}{\sqrt{2}\sigma_1}\right)dx \\ &= \int_{-\infty}^{+\infty} \frac{1}{2}\text{Erfc}\left(\frac{\sigma_0}{\sigma_1}z - \frac{m_1-m_0}{\sqrt{2}\sigma_1}\right)\frac{e^{-z^2}}{\sqrt{\pi}}dz\end{aligned} \tag{28}$$

where the second equality comes after substituting $z = \text{Erfc}^{-1}(2x)$. Moreover, by using $\text{Erfc}(x) = (2/\sqrt{\pi})\int_x^\infty e^{-w^2}dw$, and with some algebraic manipulations, (28) can be re-written as

$$\mathcal{A} = \frac{1}{\pi}\int_{-\infty}^{+\infty}\int_{\frac{\sigma_0}{\sigma_1}z - \frac{m_1-m_0}{\sqrt{2}\sigma_1}}^{+\infty} e^{-(w^2+z^2)}dwdz.$$

Now, we apply clockwise rotation to the (w, z) axis through angle θ to generate the (u, v) axis where $\tan\theta = \sigma_0/\sigma_1$, which is also equivalent to axis transformation of

$$\begin{bmatrix} u \\ v \end{bmatrix} = \begin{bmatrix} \cos\theta & -\sin\theta \\ \sin\theta & \cos\theta \end{bmatrix}\begin{bmatrix} w \\ z \end{bmatrix}.$$

This result gives

$$\begin{aligned}\mathcal{A} &= \frac{1}{\sqrt{\pi}}\int_{-\infty}^{+\infty} e^{-u^2}du\frac{1}{\sqrt{\pi}}\int_{-\frac{m_1-m_0}{\sqrt{2(\sigma_0^2+\sigma_1^2)}}}^{+\infty} e^{-v^2}dv \\ &= \frac{1}{2}\text{Erfc}\left(-\frac{m_1-m_0}{\sqrt{2(\sigma_0^2+\sigma_1^2)}}\right),\end{aligned} \tag{29}$$

where the second equality is due to $(1/\sqrt{\pi})\int_{-\infty}^{+\infty} e^{-u^2}du = 1$ and the definition of the $\text{Erfc}(\cdot)$ function. Expression (12) can be obtained from (29) by using $\text{Erfc}(-x) = 2 - \text{Erfc}(x)$.

B. General Result to Achieve Minimum $P_e(\lambda)$ in Any Channel Model

For any channel model (AWGN, Rayleigh, etc.), from [48, Property 3&4, Page 33–34], it can be seen that the ROC curve (i.e., P_d versus P_f curve) is a concave curve and is above curve "$P_d = P_f$" in a P_d versus P_f plot, which means that the complementary ROC curve (i.e., P_{md} versus P_f curve) is a convex curve and is below the curve "$P_{\text{md}} + P_f = 1$" in a P_{md} versus P_f plot. An example of the complementary ROC curve is shown in Fig. 10, in which the dashed-dotted curve is the curve "$P_{\text{md}} + P_f = 1$". In the figure, when the threshold λ increases from 0 to ∞, (P_f, P_{md}) moves along the complementary ROC curve from $(1, 0)$ to $(0, 1)$. Since the complementary ROC curve is convex and is below curve "$P_{\text{md}} + P_f = 1$", it can be concluded that when the threshold λ increases from 0 to ∞, total error rate $P_e(\lambda) = P_{\text{md}} + P_f$ first decreases (from value 1) and then increases (until value 1). So there exists one and only one point λ that minimizes $P_e(\lambda)$, which is corresponding to the point with $\frac{\partial P_e(\lambda)}{\partial\lambda} = 0$.

C. Optimal Threshold λ_e^* for AWGN Channel

For the optimal threshold, $\lambda_e^* = \arg\min_\lambda P_e(\lambda)$ is achieved when $\frac{\partial P_e(\lambda)}{\partial\lambda} = 0$. With the aid of (1), and

$$\frac{\partial}{\partial x}\text{Erfc}\left(\frac{x-l}{q}\right) = -\frac{2e^{-\frac{(x-l)^2}{q^2}}}{q\sqrt{\pi}},$$

This article has been accepted for publication in a future issue of this journal, but has not been fully edited. Content may change prior to final publication. Citation information: DOI 10.1109/TVT.2014.2381648, IEEE Transactions on Vehicular Technology

we can write

$$\frac{\partial P_e(\lambda)}{\partial \lambda} = \frac{e^{-\frac{(\lambda - N(1+\gamma)\sigma_w^2)^2}{2N(1+2\gamma)\sigma_w^4}}}{\sqrt{2\pi N(1+2\gamma)}\sigma_w^2} - \frac{e^{-\frac{(\lambda - N\sigma_w^2)^2}{2N\sigma_w^4}}}{\sqrt{2\pi N}\sigma_w^2} = 0. \quad (30)$$

After some algebraic manipulations and taking the logarithm, (30) can be simplified into a quadratic equation of λ as

$$\lambda^2 - N\sigma_w^2\lambda - \frac{N\sigma_w^4}{2}\left(N\gamma + \frac{(1+2\gamma)\ln(1+2\gamma)}{\gamma}\right) = 0.$$

Thus, the solution λ_e^* is given in (19) (here we omit the negative root since $\lambda \geq 0$).

D. Threshold Selections for Rayleigh Fading Channel

1) Threshold λ_{md}^* for Rayleigh Fading Channel: By using the Taylor series expansions of $\text{Erfc}(\alpha)$, $e^{2a\alpha}$ and $\text{Erfc}(a+\alpha)$, we can write $\overline{P_{\text{md}}^{\text{Ray}}}(\lambda)$ in (21) as

$$\overline{P_{\text{md}}^{\text{Ray}}}(\lambda) \approx \frac{1}{2}\left(1 - e^{a^2}\text{Erfc}(a)\right) - ae^{a^2}\text{Erfc}(a)\alpha + \left(\frac{a}{\sqrt{\pi}} - a^2e^{a^2}\text{Erfc}(a)\right)\alpha^2 + \mathcal{O}(\alpha^3). \quad (31)$$

Setting $\overline{P_{\text{md}}^{\text{Ray}}}(\lambda_{\text{md}}^*) = P_{\text{md}}^{\text{th}}$ for the above equation, $\lambda_{\text{md}}^*(\geq 0)$ can be selected as (22).

2) Threshold λ_e^* for Rayleigh Fading Channel: For minimum $P_e(\lambda)$, we set $\frac{\partial P_e(\lambda)}{\partial \lambda} = 0$, which can be written with the aid of (3) and (21) as

$$\frac{\partial P_e(\lambda)}{\partial \lambda} = \frac{e^{a^2+2a\alpha}\text{Erfc}\left(a+\alpha\right)}{2N\sigma_w^2\bar{\gamma}} - \frac{e^{-\alpha^2}}{\sqrt{2\pi N}\sigma_w^2} = 0 \iff e^{(a+\alpha)^2}\text{Erfc}\left(a+\alpha\right) = \sqrt{\frac{2N}{\pi}}\bar{\gamma}. \quad (32)$$

By using the Taylor series expansions of $e^{(a+\alpha)^2}$ and $\text{Erfc}\left(a+\alpha\right)$, we can write

$$e^{(a+\alpha)^2}\text{Erfc}\left(a+\alpha\right) = e^{a^2}\text{Erfc}(a) + \left[2ae^{a^2}\text{Erfc}(a) - \frac{2}{\sqrt{\pi}}\right]\alpha + \left[(1+2a^2)e^{a^2}\text{Erfc}(a) - \frac{2a}{\sqrt{\pi}}\right]\alpha^2 + \mathcal{O}(\alpha^3),$$

which can be used to solve (32). The solution is given in (23), which achieves the minimum $P_e(\lambda)$.

E. Threshold Selections for Nakagami-2 Fading Channel

1) Threshold λ_{md}^* for Nakagami-2 Fading Channel: By using the Taylor series expansions of $e^{-\alpha^2}$, $\text{Erfc}(\alpha)$, $e^{4a\alpha}$, and $\text{Erfc}(2a+\alpha)$, we can write $\overline{P_{\text{md}}^{\text{Nak}}}(\lambda)$ in (24) as

$$\overline{P_{\text{md}}^{\text{Nak}}}(\lambda) \approx \left[\frac{1}{2} - \frac{2a}{\sqrt{\pi}} + \left(4a^2 - \frac{1}{2}\right)e^{4a^2}\text{Erfc}(2a)\right] + 8a^2\left[2ae^{4a^2}\text{Erfc}(2a) - \frac{1}{\sqrt{\pi}}\right]\alpha + 4a^2\left[\left(1+8a^2\right)e^{4a^2}\text{Erfc}(2a) - \frac{4a}{\sqrt{\pi}}\right]\alpha^2 + \mathcal{O}(\alpha^3). \quad (33)$$

Setting $\overline{P_{\text{md}}^{\text{Nak}}}(\lambda_{\text{md}}^*) = P_{\text{md}}^{\text{th}}$ for the above equation, $\lambda_{\text{md}}^*(\geq 0)$ can be derived as (25).

2) Threshold λ_e^* for Nakagami-2 Fading Channel: For minimum $P_e(\lambda)$, after setting $\frac{\partial P_e(\lambda)}{\partial \lambda} = 0$ and some mathematical manipulations, we can write

$$(a+\alpha)e^{(a+\alpha)^2}\text{Erfc}(a+\alpha) = -\frac{N\bar{\gamma}^2 - 4}{4\sqrt{\pi}}.$$

By considering the Taylor series expansion of $e^{(a+\alpha)^2}$ and $\text{Erfc}(a+\alpha)$, we can write

$$\frac{2}{\sqrt{\pi}}(a+\alpha)^2 - (a+\alpha) \approx \frac{N\bar{\gamma}^2 - 4}{4\sqrt{\pi}}. \quad (34)$$

By solving the above equation, we can get λ_e^* as given in (26), which minimizes $P_e(\lambda)$.

REFERENCES

[1] ECMA-International, "MAC and PHY for operation in TV white space," Jun. 2012. [Online]. Available: http://www.ecma-international.org/publications/files/ECMA-ST/ECMA-392.pdf

[2] C. Cordeiro, K. Challapali, D. Birru, and N. Sai Shankar, "IEEE 802.22: An introduction to the first wireless standard based on cognitive radios," *Journal of Communications (JCM)*, vol. 1, no. 1, pp. 38–47, Apr. 2006.

[3] S. J. Shellhammer, "Spectrum sensing in IEEE 802.22," in *1st IAPR Workshop on Cognitive Information Processing*, 2008.

[4] C. Stevenson, G. Chouinard, Z. Lei, W. Hu, S. Shellhammer, and W. Caldwell, "IEEE 802.22: The first cognitive radio wireless regional area network standard," *IEEE Commun. Mag.*, vol. 47, no. 1, pp. 130 –138, Jan. 2009.

[5] H. Urkowitz, "Energy detection of unknown deterministic signals," *Proc. of the IEEE*, vol. 55, no. 4, pp. 523–531, Apr. 1967.

[6] F. F. Digham, M. S. Alouini, and M. K. Simon, "On the energy detection of unknown signals over fading channels," *IEEE Trans. Commun.*, vol. 55, no. 1, pp. 21–24, Jan. 2007.

[7] S. Herath, N. Rajatheva, and C. Tellambura, "Energy detection of unknown signals in fading and diversity reception," *IEEE Trans. Commun.*, vol. 59, no. 9, pp. 2443–2453, Sep. 2011.

[8] S. Atapattu, C. Tellambura, and H. Jiang, "Performance of an energy detector over channels with both multipath fading and shadowing," *IEEE Trans. Wireless Commun.*, vol. 9, no. 12, pp. 3662–3670, Dec. 2010.

[9] S. Atapattu, C. Tellambura, and H. Jiang, "Energy detection based cooperative spectrum sensing in cognitive radio networks," *IEEE Trans. Wireless Commun.*, vol. 10, no. 4, pp. 1232–1241, Apr. 2011.

[10] P. Cheraghi, Y. Ma, R. Tafazolli, and Z. Lu, "Cluster-based differential energy detection for spectrum sensing in multi-carrier systems," *IEEE Trans. Signal Processing*, vol. 60, no. 12, pp. 6450–6464, Dec. 2012.

[11] D. Ramirez, J. Via, and I. Santamaria, "The locally most powerful test for multiantenna spectrum sensing with uncalibrated receivers," in *Proc. IEEE ICASSP*, Mar. 2012, pp. 3437–3440.

[12] J. Sala-Alvarez, G. Vazquez-Vilar, and R. Lopez-Valcarce, "Multiantenna GLR detection of rank-one signals with known power spectrum in white noise with unknown spatial correlation," *IEEE Trans. Signal Processing*, vol. 60, no. 6, pp. 3065–3078, Jun. 2012.

[13] F. Lin, R. Qiu, Z. Hu, S. Hou, J. Browning, and M. Wicks, "Generalized FMD detection for spectrum sensing under low signal-to-noise ratio," *IEEE Commun. Lett.*, vol. 16, no. 5, pp. 604–607, May 2012.

[14] Z. Zhang, Z. Han, H. Li, D. Yang, and C. Pei, "Belief propagation based cooperative compressed spectrum sensing in wideband cognitive radio networks," *IEEE Trans. Wireless Commun.*, vol. 10, no. 9, pp. 3020–3031, Sep. 2011.

[15] M. Derakhshani, T. Le-Ngoc, and M. Nasiri-Kenari, "Efficient cooperative cyclostationary spectrum sensing in cognitive radios at low SNR regimes," *IEEE Trans. Wireless Commun.*, vol. 10, no. 11, pp. 3754–3764, Nov. 2011.

[16] T. Cui, F. Gao, and A. Nallanathan, "Optimization of cooperative spectrum sensing in cognitive radio," *IEEE Trans. Veh. Technol.*, vol. 60, no. 4, pp. 1578–1589, May 2011.

[17] L. Wei, P. Dharmawansa, and O. Tirkkonen, "Multiple primary user spectrum sensing in the low SNR regime," *IEEE Trans. Commun.*, vol. 61, no. 5, pp. 1720–1731, May 2013.

[18] Y. Feng, B. Jiao, and L. Song, "Satellite-based spectrum sensing for dynamic spectrum sharing in ground-located CRNs," *Wireless Personal Communications*, vol. 57, no. 1, pp. 105–117, Mar. 2011.

[19] T. Wang, L. Song, Z. Han, and W. Saad, "Overlapping coalitional games for collaborative sensing in cognitive radio networks," in *Proc. IEEE WCNC 2013*, pp. 4118–4123.
[20] T. Yucek and H. Arslan, "A survey of spectrum sensing algorithms for cognitive radio applications," *IEEE Communications Surveys & Tutorials*, vol. 11, no. 1, pp. 116–130, First Quarter 2009.
[21] Y. Chen, "Improved energy detector for random signals in Gaussian noise," *IEEE Trans. Wireless Commun.*, vol. 9, no. 2, pp. 558–563, Feb. 2010.
[22] O. Olabiyi, S. Alam, O. Odejide, and A. Annamalai, "Further results on the energy detection of unknown deterministic signals over generalized fading channel," in *Proc. IEEE GLOBECOM'11 Workshops*, pp. 908-912.
[23] Z. Quan, S. Cui, A. H. Sayed, and H. V. Poor, "Optimal multiband joint detection for spectrum sensing in cognitive radio networks," *IEEE Trans. Signal Process.*, vol. 57, no. 3, pp. 1128–1140, Mar. 2009.
[24] W.-Y. Lee and I. F. Akyildiz, "Optimal spectrum sensing framework for cognitive radio networks," *IEEE Trans. Wireless Commun.*, vol. 7, no. 10, pp. 3845–3857, Oct. 2008.
[25] Y.-C. Liang, Y. Zeng, E. Peh, and A. T. Hoang, "Sensing-throughput tradeoff for cognitive radio networks," *IEEE Trans. Wireless Commun.*, vol. 7, no. 4, pp. 1326–1337, Apr. 2008.
[26] S. Ciftci and M. Torlak, "A comparison of energy detectability models for spectrum sensing," in *Proc. IEEE GLOBECOM 2008*.
[27] F. Shayegh and F. Labeau, "On signal detection in the presence of weakly correlated noise over fading channels," *IEEE Trans. Commun.*, vol. 62, no. 3, pp. 797–809, Mar. 2014.
[28] R. Fan and H. Jiang, "Optimal multi-channel cooperative sensing in cognitive radio networks," *IEEE Trans. Wireless Commun.*, vol. 9, no. 3, pp. 1128–1138, Mar. 2010.
[29] Q. Peng, P. Cosman, and L. Milstein, "Optimal sensing disruption for a cognitive radio adversary," *IEEE Trans. Veh. Technol.*, vol. 59, no. 4, pp. 1801–1810, May 2010.
[30] S. Atapattu, C. Tellambura, and H. Jiang, "Spectrum sensing via energy detector in low SNR," in *Proc. IEEE Int. Conf. Commun. (ICC)*, Jun. 2011.
[31] R. Mills and G. Prescott, "A comparison of various radiometer detection models," *IEEE Trans. Aerosp. Electron. Syst.*, vol. 32, no. 1, pp. 467–473, Jan. 1996.
[32] I. S. Gradshteyn and I. M. Ryzhik, *Table of Integrals, Series, and Products*, 6th ed. Academic Press, Inc., 2000.
[33] S. Atapattu, C. Tellambura, and H. Jiang, "A mixture gamma distribution to model the SNR of wireless channels," *IEEE Trans. Wireless Commun.*, vol. 10, no. 12, pp. 4193–4203, Dec. 2011.
[34] A. P. Prudnikov, Y. A. Brychkov, and O. I. Marichev, *Integrals and Series, vol. 2*. Gordon and Breach science Publishers, 1986.
[35] S. Atapattu, C. Tellambura, and H. Jiang, "Analysis of area under the ROC curve of energy detection," *IEEE Trans. Wireless Commun.*, vol. 9, no. 3, pp. 1216–1225, Mar. 2010.
[36] H. L. V. Trees, *Detection, Estimation, and Modulation Theory, Part I*. Wiley-Interscience, 2001.
[37] W. Zhang, R. Mallik, and K. B. Letaief, "Optimization of cooperative spectrum sensing with energy detection in cognitive radio networks," *IEEE Trans. Wireless Commun.*, vol. 8, no. 12, pp. 5761–5766, Aug. 2009.
[38] J. Shen, Y. Liu, S. Liu, J. Gao, G. Xie, and C. Chi, "Robust energy detection based on Bayesian estimation for cognitive radio," in *Proc. IEEE GLOBECOM 2008*.
[39] F. Penna, Y. Sun, L. Dolecek, and D. Cabric, "Joint spectrum sensing and detection of malicious nodes via belief propagation," in *Proc. IEEE GLOBECOM 2011*.
[40] P. Jia, M. Vu, T. Le-Ngoc, S.-C. Hong, and V. Tarokh, "Capacity- and Bayesian-based cognitive sensing with location side information," *IEEE J. Select. Areas Commun.*, vol. 29, no. 2, pp. 276–289, Feb. 2011.
[41] A. Singh, M. Bhatnagar, and R. Mallik, "Cooperative spectrum sensing in multiple antenna based cognitive radio network using an improved energy detector," *IEEE Commun. Lett.*, vol. 16, no. 1, pp. 64–67, Jan. 2012.
[42] D. Cabric, A. Tkachenko, and R. W. Brodersen, "Experimental study of spectrum sensing based on energy detection and network cooperation," in *Proc. 1st Int. workshop on Technology and Policy for Accessing Spectrum (TAPAS)*, Aug. 2006.
[43] "IEEE standard for terminology and test methods for analog-to-digital converters," *IEEE Std 1241-2010 (Revision of IEEE Std 1241-2000)*, pp. 1–139, Jan. 2011.
[44] A. Verma and B. Razavi, "A 10-bit 500-MS/s 55-mW CMOS ADC," *IEEE J. Solid-State Circuits*, vol. 44, no. 11, pp. 3039–3050, Nov. 2009.
[45] T.-H. Yu, O. Sekkat, S. Rodriguez-Parera, D. Markovic, and D. Cabric, "A wideband spectrum-sensing processor with adaptive detection threshold and sensing time," *IEEE Trans. Circuits and Systems*, vol. 58, no. 11, pp. 2765–2775, Nov. 2011.
[46] R. Tandra and A. Sahai, "SNR Walls for Signal Detection," *IEEE Journal of Selected Topics in Signal Processing*, vol. 2, no. 1, pp. 4–17, Feb. 2008.
[47] S. S. Kalamkar, A. Banerjee, and A. K. Gupta, "SNR wall for generalized energy detection under noise uncertainty in cognitive radio," in *Proc. 19th Asia-Pacific Conference on Communications (APCC)*, pp. 375-380, 2013.
[48] B. C. Levy, *Principles of Signal Detection and Parameter Estimation*, Springer, 2008

Saman Atapattu (S'06-M'14) received the B.Sc. degree in electrical and electronics engineering from the University of Peradeniya, Sri Lanka in 2003, the M.Eng. degree in telecommunications from Asian Institute of Technology (AIT), Thailand in 2007, and the Ph.D. degree in electrical engineering from the University of Alberta, Canada in 2013.

He is currently a research fellow at the Department of Electrical and Computer System Engineering, Monash University, Australia. His research interests include cooperative communications, cognitive radio networks, energy harvesting, and performance analysis of communication systems.

Chintha Tellambura (F'11) received the B.Sc. degree (with first-class honor) from the University of Moratuwa, Sri Lanka, in 1986, the M.Sc. degree in Electronics from the University of London, U.K., in 1988, and the Ph.D. degree in Electrical Engineering from the University of Victoria, Canada, in 1993.

He is currently a Professor with the Department of Electrical and Computer Engineering, University of Alberta. His research interests focus on communication theory dealing with the wireless physical layer.

Prof. Tellambura was an Associate Editor for the IEEE TRANSACTIONS ON COMMUNICATIONS and the Area Editor for Wireless Communications Systems and Theory in the IEEE TRANSACTIONS ON WIRELESS COMMUNICATIONS.

Hai Jiang (M'07) received the B.Sc. and M.Sc. degrees in Electronics Engineering from Peking University, Beijing, China, in 1995 and 1998, respectively, and the Ph.D. degree in electrical engineering from the University of Waterloo, Waterloo, Ontario, Canada, in 2006.

He is currently an Associate Professor at the Department of Electrical & Computer Engineering, University of Alberta, Canada. His research interests include radio resource management, cognitive radio networking, and cross-layer design for wireless multimedia communications.

Nandana Rajatheva (SM'01) received the B.Sc. degree in electronics and telecommunication engineering (with first-class honors) from the University of Moratuwa, Moratuwa, Sri Lanka, in 1987, and the M.Sc. and Ph.D. degrees from the University of Manitoba, Winnipeg, MB, Canada, in 1991 and 1995, respectively. He was with the School of Engineering and Technology, Asian Institute of Technology, Pathumthani, Thailand (1996–2001, 2005–2010) where he holds a visiting position now. Currently, he is an Adjunct Professor with the Department of Communication Engineering, University of Oulu, Oulu, Finland.

His research interests include signal processing, performance analysis, resource allocation for massive MIMO, relay, cognitive radio, and hierarchical cellular systems.